



Damage of Saturated Rocks Undergoing Triaxial Deformation Using Complex Electrical Conductivity Measurements: Experimental Results

P. W. J. Glover^{1,3}, J. B. Gómez², P. G. Meredith¹, K. Hayashi³, P. R. Sammonds¹ and S. A. F. Murrell

¹Department of Geological Sciences, University College London, Gower St., London WC1E 6BT, U.K.

²Departamento de Geología, Universidad de Zaragoza, Pza. San Francisco s/n, 50009 Zaragoza, Spain

³Institute of Fluid Sciences, Tohoku University, 2-1-1 Katahira, Aoba-ku, Sendai 980-77, Japan

Received 10 May 1996; accepted 11 June 1997

Abstract. The frequency dependent complex electrical conductivity of brine saturated rocks is extremely sensitive to changes in the volume, connectivity, orientation, and surface topography of pores and cracks. We have made triaxial deformation experiments on sandstone specimens saturated with distilled water. Experiments were carried out for several values of confining pressure, and in both drained and undrained regimes. During the deformation the full complex (in-phase and out-of-phase) electrical parameter set was measured (i.e. conductivity, resistivity, permittivity etc.) for 50 frequencies from 20 Hz to 1 MHz. Only the data at 1 kHz will be discussed here. This data tracks how the rock undergoes crack closure, followed by dilatancy, crack linking, and finally failure, as axial strain is increased. The data indicates well how early the formation of new cracks begins, showing that the quasi-linear portion of the stress-strain curve for triaxial deformation of saturated rocks does not represent truly elastic behaviour, but represents the combined effects of crack closure perpendicular to the strain axis and the formation of tensile cracks parallel to the strain axis. The electrical data has also been used to derive an electrical-equivalent change in porosity, and to examine the way that the cementation exponent and the tortuosity of the pore and crack network change during deformation.

© 1997 Published by Elsevier Science Ltd

1 Introduction

There have been relatively few studies of the complex electrical properties of rocks compared to the number of studies concerning seismic and hydraulic properties. This is quite surprising considering the potential information that electrical data can provide on evolving rock micro-structure. The main reason for this has been the relative difficulty in making accurate electrical conductivity meas-

urements. Frequency dependent complex electrical conductivity in hydrostatically confined rocks has been measured by Lockner and Byerlee (1985). The effect of the rock micro-structure on electrical properties has been studied by Ruffet et al. (1991), while Revil and Glover (1997) have concentrated on surface conduction, and Freund and Nover (1995) have examined the complex electrical conductivity of KTB samples. There are some measurements done during uniaxial deformation (Glover et al., 1994b), but no previous work on rocks during triaxial deformation, that we are aware of. Here, and in Glover et al. (1996), we examine the complex electrical properties of water saturated sandstones during triaxial deformation.

2 Experimental procedure and samples

Darley Dale sandstone was used for all triaxial experiments. This is a well indurated, granular, feldspathic quartz sandstone with 75% quartz, 15% feldspar (plagioclase and microcline), and 10% muscovite/illite. It is poorly graded with grain sizes in the range 0.08-0.8 mm, has a medium to high porosity (12-28%), and a high permeability (500-2000 mD). Measurements were performed on right cylinders 40 mm in diameter, and approximately 110 mm in length. Axial end surfaces were ground flat and parallel. Each sample was saturated with initially pure deionised water that had been degassed by vacuum for 24 hours prior to use (Glover et al., 1994a). Deionised water was chosen to facilitate more accurate surface conduction measurements made as a function of frequency, which are not discussed in this paper due to length constraints.

Complex electrical parameter measurements were made using a specially designed two electrode cell (Glover et al., 1996) and a 150 tonne load frame with a 400 MPa pressure vessel. The electrodes were made from platinum-blackened platinum gauze (Glover et al., 1994a). It was found that,

Correspondence to: P.W.J. Glover

Table 1. Test Information

Sample	Regime	Confining Pressure, MPa	Peak Axial Stress, MPa	Axial Strain at Peak Stress, %	Axial Stress at Failure, MPa	Axial Strain at Failure, %	Initial Porosity, %	Initial In Phase Resistivity, ohm.m	Initial Out-of-Phase Resistivity, ohm.m
TRY1	Undrained	50	141.7	1.74	103.2	2.08	28.0	1397.00	28.71
TRY2	Undrained	25	111.8	1.51	95.6	1.68	23.4	1735.84	21.91
TRY4	Drained	50	203.5	1.73	185.3	1.89	15.9	4016.72	50.87

providing they were well blacked, two electrodes produced negligible electrode polarisation between 20 Hz and 1 MHz, and were easier to incorporate into a cell designed to apply axial stresses to the rock sample. We made complex conductivity measurements as a function of frequency, from 20 Hz to 1 MHz, using a computer controlled HP4284A impedance bridge. The computer makes lead corrections to the data, converts the measured complex conductances into specific measurements (complex conductivity), calculates other electrical parameters (e.g. complex resistivities and permittivities), and logs the data. Only the data at 1 kHz will be used in this paper. This frequency was chosen as that at which the out-of-phase conductivity is minimized, which allows the data to be a function of the pore and crack fluid volume, with contributions from surface conduction reduced to negligible levels.

Initially a hydrostatic confining pressure of either 25 MPa or 50 MPa was applied in stages, while monitoring changes in the complex electrical conductivity from 20 Hz to 1 MHz. Triaxial deformation was then started at a constant strain rate ($1.66 \times 10^{-6} \text{ s}^{-1}$ for all samples) until failure occurred, during which the complex electrical conductivity continued to be monitored. Both drained and undrained tests were carried out. In the drained tests the pore fluid was allowed to drain freely to atmospheric pressure through electrically insulated pipework, where it was collected in a measuring cylinder. The measuring cylinder was arranged on an electronic balance in such a way that the expelled/imbibed fluid volume could be measured gravimetrically. This information was used to calculate the change in volumetric porosity, and also combined with electrical data to derive the cementation exponent, m , and tortuosity, τ , during deformation.

3 Complex resistivity during triaxial deformation

Figures 1 to 3 show the variation of the complex resistivity at 1 kHz and measured stress-strain curves for the three samples of Darley Dale sandstone (summarised in Table 1) as they were triaxially deformed until failure. Sample TRY4 was drained to atmospheric pressure, and the volumetric changes in the cracks and pores were monitored by measuring the mass of fluid expelled/imbibed during the experiment. The variation of the complex electrical behaviour at 1 kHz during deformation has a generic behaviour. At low values of axial strain the primary

process operating in the rock is compaction of pores and cracks. Pores and cracks that are most sensitive to closure are those with (i) low aspect ratios, and (ii) orientations perpendicular to the direction of principal stress. The relatively low levels of confining pressure used in these tests result in the direction of principal stress being almost axial for the majority of the deformation. The dominating process at low strains, therefore, is the closure of cracks perpendicular to the direction of principal stress and the axis of the sample. Closure of these cracks has little effect on the saturated rock electrical conductivity because they are perpendicular to the direction of current flow, and their loss provides only a small change in the tortuosity of the current flow paths. The resulting effect of this closure is a small increase in the saturated rock electrical resistivity.

New cracks begin to grow at some value of axial strain in the region before the resistivity curves reach their peak value. These cracks are aligned in a direction preferentially parallel to the direction of principal stress, and have a large effect on the saturated rock electrical conductivity because, at such low values of confining pressure, they are formed roughly in the same direction as the current flow. The maximum of the broad peak in the electrical resistivity curve represents the strain at which the effect on electrical conductivity due to crack closure is exactly equalled by the effect of new crack formation. Note that it occurs well inside the quasi-elastic region of the stress-strain curve. This shows very well that it is wrong to think of the linear portion of the stress-strain curve for rocks as representing truly elastic behaviour. Rather it is the outcome of two competing mechanisms; (i) the closure of a crack population perpendicular to the axis of deformation, and (ii) the growth and propagation of a population of cracks aligned with the axis of the deforming sample.

It should be noted that it is also possible for the formation of new cracks to enable further compaction. For even greater axial strains, the effect of new cracks upon the electrical properties of the saturated rocks begins to dominate. The resistivity decreases sharply due to the combined effect of cracks growing in the same general direction as the current flow, and an ever increasing connectivity as cracks inter-link. Eventually crack linking becomes commonplace, dramatically reducing the tortuosity of current flow, and hence electrical resistivity, which continues until failure. Dynamic rock failure occurs by fracture localization when sufficient cracks coalesce along a plane intersecting the sample diagonally. At failure the stress drops to a lower level representing that needed to

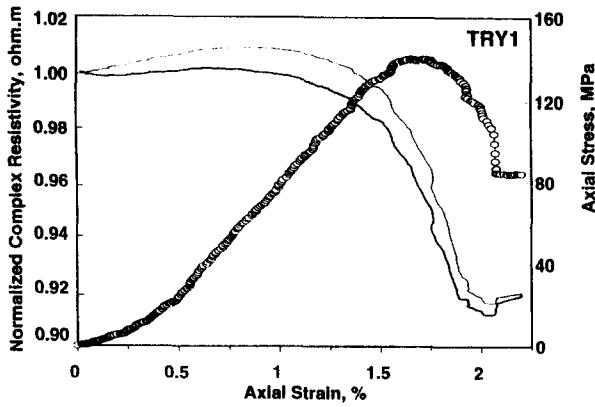


Fig.1. Normalised complex resistivity at 1 kHz (thin solid line, in-phase resistivity; thick solid line, out-of-phase resistivity) and applied axial stress (triangles) as a function of axial strain during triaxial deformation until failure for Darley Dale sandstone (TRY1).

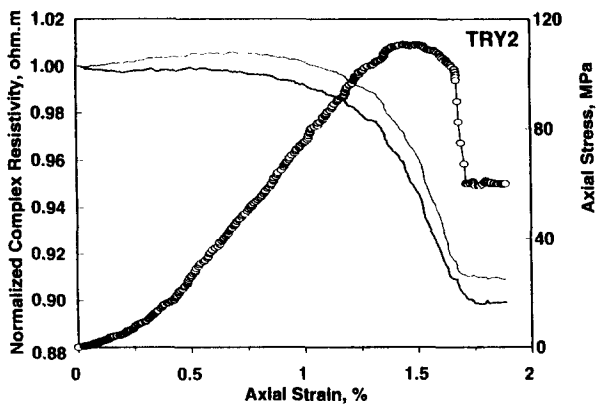


Fig.2. Normalised complex resistivity at 1 kHz (thin solid line, in-phase resistivity; thick solid line, out-of-phase resistivity) and applied axial stress (triangles) as a function of axial strain during triaxial deformation until failure for Darley Dale sandstone (TRY2).

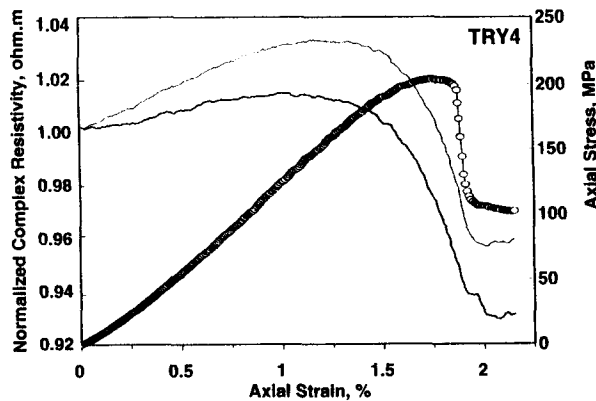


Fig.3. Normalised complex resistivity at 1 kHz (thin solid line, in-phase resistivity; thick solid line, out-of-phase resistivity) and applied axial stress (triangles) as a function of axial strain during triaxial deformation until failure for Darley Dale sandstone (TRY4).

cause deformation by frictional shearing along the fractures. It might have been expected that there would be a large decrease in resistivity at failure due to the sudden formation of a few major fluid saturated fractures with large conductivities. This does not occur in these experiments although we would expect it to be the case for experiments on low porosity saturated crystalline rock samples. In this case, conduction through the pore structure of the rock between developing major cracks remains high throughout the deformation due to the highly porous nature of Darley Dale sandstone. Hence, the electrical properties of the rock experience the effect of new crack growth throughout the whole process of deformation rather than all at once when the cracks link up at failure.

4 Porosity during triaxial deformation

The porosity of sample TRY4 was measured during the initial application of 50 MPa confining pressure and during the subsequent deformation. This was done by combining the change in crack and pore volume derived from the gravimetric data with the initial porosity of the rock. This porosity we will term the *volumetric porosity*, since the temperature was constant in all of our experiments. The porosity of all samples can also be calculated from the electrical data by assuming Archie's law holds,

$$\sigma_r(\nu, \epsilon) = \sigma_f(\nu, \epsilon) \cdot \phi(\epsilon)^{m(\epsilon)}, \quad (1)$$

where $\sigma_r(\nu, \epsilon)$ is the conductivity of the saturated rock at a given frequency, ν , and axial strain, ϵ . The symbol $\sigma_f(\nu)$ is the conductivity of the pore-fluid at the same frequency, and ϕ is a porosity. The cementation exponent is m , and lies between 1.5 and 2.5 for sandstones. We will call the porosity calculated from Eq. (1) with a constant cementation exponent ($=2$) as the *electrical porosity*. It is important to make the distinction between the two, not only because the electrical porosity contains significant assumptions in its derivation, but because it measures a different physical porosity. The volumetric porosity represents the hydraulically connected porosity as it is usually understood, while the electrical porosity represents the electrically connected porosity, and is implicitly weighted to favour both cracks that align axially and new crack growth or crack propagation that tends to increase the pore and crack network connectivity. This gives us the potential for using electrical data to produce a useful crack damage parameter, as the mechanical properties of a rock under triaxial conditions are also most sensitive crack formation in the axial direction, and crack formation that tends to increase the connectivity of the crack network (see the companion paper, Gómez et al., this volume).

Figure 4 shows the variation in the volumetric and electrical porosity of sample TRY4 as the deformation progressed. The electrical porosity is higher than the volumetric porosity, which is likely to be the result of the electrical connectivity being greater than the hydraulic connectivity, but may also be due to a failure in the assumptions made in deriving the electrical porosity. However, the shape of the porosity curve as a function of deformation for both methods is very similar. At low strains the porosity decreases as cracks perpendicular to the axis are closed. At higher strains the porosity increases due to the formation and propagation of cracks oriented parallel to the axis. After failure there is no macroscopic change in the porosity of the sample.

5 Cementation exponent during triaxial deformation

For all samples we have measured the complex electrical conductivity as a function of frequency and axial strain, as well as the electrical conductivity of the saturating fluid as a function of frequency using techniques described in Glover *et al.* (1994a). Additionally, for sample TRY4, we have an independent measurement of the porosity of the rock as a function of deformation calculated from gravimetric fluid expulsion/imbibition measurements. These three parameters can be used with Eq.(1) to calculate the cementation exponent during deformation, as shown in Fig. 4.

High values of the cementation exponent (≥ 2) are associated with pores of equant geometry, while small values, approaching unity, are associated with long thin cracks. At low axial stresses the cementation exponent was found to increase from its initial pre-deformation (50 MPa hydrostatic) value of 1.932, which is near 2 and consistent with a highly porous saturated sedimentary rock with a small number of thin cracks interacting with a background porous matrix. At low axial stresses the cementation exponent was found to increase. This is consistent with our previous interpretations of the variation of electrical resistivity and porosity, and represents the closure of thin high aspect ratio cracks aligned perpendicular to the direction of principal stress. As the high aspect ratio cracks close, they leave the pore and crack network more dominated by equant pores, which close only grudgingly upon application of either hydrostatic or axial stresses. Thus the value of the cementation exponent increases. The increase in the value of the cementation exponent continues while the electrical resistivity increases, and reaches a peak at a value of axial strain between that at which the complex resistivity reaches its peak value and that at which the peak stress occurs. This is the value of axial strain where the change in the cementation exponent due to closure of thin cracks arranged perpendicular to the direction of stress and conductivity measurement is the same as that due to the formation of new cracks oriented

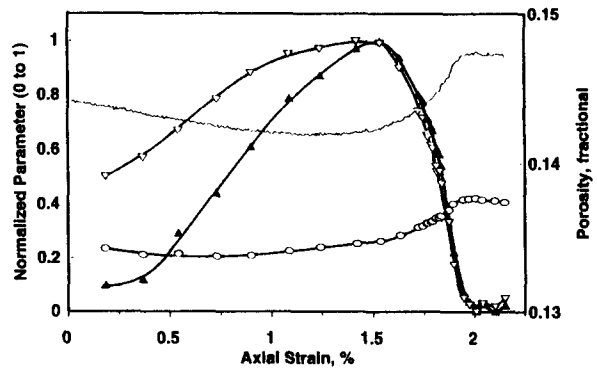


Fig.4. Comparison of micro-structural parameters during triaxial deformation for TRY4. Thin solid line, electrical porosity; circles, volumetric porosity; solid triangles, cementation exponent; open triangles, tortuosity. Cementation exponent and tortuosity normalised to lie between 0 and 1.

sub-parallel to the axis of deformation and conductivity measurement. The formation and growth of these cracks results in the reduction of the cementation exponent once more. As axial strain increases further the cementation exponent decreases swiftly due to the proliferation of new cracks forming and propagating sub-parallel to the axis of deformation, until its value becomes constant after failure, where the deformation is localised along a single diagonal fracture plane.

6 Tortuosity and connectivity during triaxial deformation

Electrical conductivity data can also be used to calculate the tortuosity and connectivity of the pore and crack matrix as the rock is deformed using an approach also based upon Archie's law. Rearranging Eq. (1) gives,

$$F(\nu, \epsilon) = \frac{\sigma_f(\nu)}{\sigma_r(\nu, \epsilon)} = \phi(\epsilon)^{-m(\nu, \epsilon)}, \quad (2)$$

where $F(\nu, \epsilon)$ is the formation factor. Here the conductivities both depend upon frequency, ν , and that of the saturated rock also depends upon deformation, represented by the axial strain, ϵ . We can remove the frequency dependence in this equation by choosing a single frequency where out-of-phase conduction is minimized (1 kHz).

There exists a relationship between the formation factor and the tortuosity of a rock that can be derived by remembering that a rock which has uninterrupted fluid paths through it has a cementation exponent equal to unity (Guéguen and Palciauskas, 1992). So for a rock with no tortuosity, the formation factor scales with the inverse porosity, ϕ^{-1} . Thus if we have a rock which has a finite non-zero tortuosity, the formation factor from Eq. (2) can be expressed as,

$$F(\varepsilon) = \phi(\varepsilon)^{-1} \cdot \phi(\varepsilon)^{1-m(\varepsilon)}, \quad (3)$$

where the first term represents the effect of the volume of the pore and crack space on the conductivity and formation factor of the rock *without* taking into account the way pores and cracks are arranged within the rock. The second term expresses the remaining effect, i.e. that of the geometrical arrangement of pores and cracks of a given total volume. It is the second term that is called the electrical tortuosity. We can rewrite Eq. (3) as,

$$F(\varepsilon) = \frac{\sigma_f}{\sigma_r(\varepsilon)} = \frac{\alpha(\varepsilon)}{\phi(\varepsilon)}, \quad (4)$$

where α is the electrical tortuosity, and ϕ is the porosity of the rock (Ruffet et al., 1991). We can calculate the electrical tortuosity during deformation since we know (i) the conductivity of the pore fluid, (ii) the conductivity of the rock at any axial strain, ε , and (iii) we have an *independent* measure of the porosity of the rock during deformation. The electrical connectivity is simply the reciprocal of the tortuosity.

Figure 4 also shows the variation of electrical tortuosity as a function of axial strain during the drained triaxial deformation of sample TRY4. At low axial strains the tortuosity increases due to the compactive loss of paths for electrical transport. As axial strain increases further new cracks begin to form, and their effect is to reduce the overall tortuosity of the network. The tortuosity curve reaches a maximum when the effect on tortuosity by the compacting cracks, and by the growing cracks balance each other out. Note that the position of this maximum occurs at an axial strain that is greater than the axial strain at which the porosity curves have their minimum (Fig. 4), and greater than the axial strain at which the resistivity curves (Figs. 1 to 3) have their maximum. This comparison shows that the development of large scale connectivity in the rock occurs late in deformation compared to when new cracking begins to have a dominating effect on both the volume of the crack and pore network, and the electrical parameters of the saturated rock. This indicates that even at large axial strains the mechanism of crack closure perpendicular to the axis of the sample is controlling the tortuosity, because the loss of perpendicular cracks impairs the ability of the new axially oriented cracks from forming a highly interconnected crack network. Eventually the tortuosity decreases substantially as the new cracking becomes dominant, and gross crack inter-linking occurs just prior to failure. After failure the tortuosity remains constant. It should be noted that the tortuosity and the cementation exponent curves peak at the same value of axial strain. This is because the tortuosity term of Eq. (3) depends on the cementation exponent.

7 Conclusions

Measurement of the complex electrical parameters of saturated rocks during triaxial deformation has the potential for giving much useful information concerning the closure and subsequent formation and growth of new cracks that alter the rock micro-structure. It is particularly useful as it is sensitive to the orientation of the cracks that are closing, opening or propagating. Specifically, the examination of electrical parameters, and micro-structural characteristics derived from them leads us to the following conclusions:

1. The onset of new crack formation occurs well inside the quasi-linear part of the stress-strain curve.
2. The quasi-linear portion of the stress-strain curve is the result of competition between closure of one population of cracks oriented perpendicular to the axis, and the growth of new and propagation of existing cracks parallel to the axis.
3. The relative importance of crack closure and dilatation during deformation controls the observed volumetric porosity, electrical porosity, cementation exponent, tortuosity, and the resulting electrical data.
4. The development of large scale connectivity (indicated by large drops in tortuosity) is observed to be confined to just prior to failure.

Clearly there is an urgent need for similar experiments to be done, measuring not only the electrical parameters axially, but also for two perpendicular radial directions. Such a data set would be able to observe the development of connectivity within the rock much more rigorously.

References

- Freund, D. and Nover, G., Hydrostatic pressure tests for the permeability-formation factor relation on crystalline rocks from the KTB drilling project, *Surv. Geophys.* 16, 37-50, 1995.
- Glover, P.W.J., Meredith, P.G., Sammonds, P.R., and Murrell, S.A.F., Ionic surface electrical conductivity in sandstone, *J. Geophys. Res.* 99, 21635-21650, 1994a.
- Glover, P.W.J., Meredith, P.G., Sammonds, P.R., and Murrell, S.A.F., Measurements of complex electrical conductivity and fluid permeability in porous rocks at raised confining pressures, *In Rock Mechanics in Petroleum Engineering*, Proceedings of EUROCK '94, SPE/ISRM International Meeting, Delft, The Netherlands, Balkema, Amsterdam, pp 29-36, 1994b.
- Glover, P.W.J., Gómez, J.B., Meredith, P.G., Boon, S.A., Sammonds, P.R., and Murrell, S.A.F., Modelling the stress-strain behaviour of saturated rocks undergoing triaxial deformation using complex electrical conductivity measurements, *Surv. Geophys.* 17(3), 307-330, 1996.
- Guéguen, Y. and Palciauskas, V., *Introduction à la physique des roches*, Hermann, Paris, ISBN 2705661380, 1992.
- Lockner, D.A. and Byerlee, J.D., Complex resistivity measurements of confined rock, *J. Geophys. Res.* 90, 7837-7847, 1985.
- Revil, A. and Glover, P.W.J., A theory of ionic electrical conduction in porous media, *Phys. Rev. B.* 55, 1757-1773, 1997.
- Ruffet, C., Guéguen, Y., and Darot, M., Complex conductivity measurements and fractal nature of porosity, *Geophysics* 56, 758-768, 1991.